Seven-equation, two-phase flow three-dimensional calculations using a Mixed-Element-Volume method

Stephen F. Wornom, Bruno Koobus, Hervé Guillard, Angelo Murrone, Alain Dervieux

INSTITUT NATIONAL DE RECHERCHE EN INFORMATIQUE ET EN AUTOMATIQUE

Seven-equation, two-phase flow three-dimensional calculations using a Mixed-Element-Volume method

S. Wornom, B. Koobus, H. Guillard, A. Murrone, A. Dervieux

N° 5560

April 2005

Thème NUM

ISSN 0249-6399

Seven-equation, two-phase flow three-dimensional calculations using a Mixed-Element-Volume method

S. Wornom*, B. Koobus†, H. Guillard‡, A. Murrone§, A. Dervieux¶

Thème NUM — Systèmes numériques
Projet Smash

Rapport de recherche n° 5560 — April 2005 — 25 pages

Abstract: We present the extension of the five-equation two-dimensional two-phase model of Guillard and Murrone to three-dimensions. The Riemann solver is the acoustic version of the one proposed by Guillard and Murrone. The numerical scheme is a Mixed-Element-Volume approximation centered on the vertices of tetrahedra. It uses an edge based formulation. Upstream-Downstream tetrahedra-based limiters are applied for positiveness reinforcement. The computation in advanced in time using explicit multi-stage schemes. This numerical technology is implemented in the parallel mode using mesh partitioning and the message passing interface (MPI). We present some preliminary computations for validation with respect to 2D results and an application to the action of a blast wave on a dense bubble.

Key-words: Computational fluid dynamics, two-phase flow

* INRIA, 2004 Route des Lucioles, BP. 93, 06902 Sophia-Antipolis, France
† Dept Mathématiques, CC.051 34095 MONTPELLIER Cedex 5, France
‡ INRIA, 2004 Route des Lucioles, BP. 93, 06902 Sophia-Antipolis, France
§ INRIA, 2004 Route des Lucioles, BP. 93, 06902 Sophia-Antipolis, France
¶ INRIA, 2004 Route des Lucioles, BP. 93, 06902 Sophia-Antipolis, France

Calcul d'écoulements diphasiques avec la méthode mixte-élément-volume

Résumé : On présente l'extension du modèle diphasique à cinq équations de Guillard et Murrone au cas tridimensionnel. Le solveur de Riemann approché choisi est la version du solveur proposé par Guillard et Murrone. Le schéma numérique est une approximation Mixte-Elément-Volume centrée sur les sommets d'une tétraèdrisation. Il utilise une formulation basée sur les arètes. Des limiteurs par tétraèdres amont et aval garantissent de bonne propriétés de positivité. L'avancement en temps est explicite multi-pas. Cette technologie numérique est implémentée en mode parallèle par partition et passage de messages. On présente des premiers calculs de validation par rapport aux calculs 2D et une application à l'action d'un choc incident sur une bulle dense.

Mots-clés : Mécanique des fluides numérique, écoulement multi-phase

1 Introduction

Numerical methods for multi-fluid or multiphase flows have a long history and many different methods have become successively popular over the last five decades. Today Eulerian formulations are favoured for solving many problems where the interface shows strong variations. The difficulties are not only related with the advection of the interface, but also the computation of the composite fluid. The diffuse interface method of Saurel and Abgrall [19] is an Eulerian method which applies particularly to the latter problem. The main principle of this method is to build accurate and stable models for the mixed cells involving fluids with very different properties. Then such methods can be modeled in the same manner as an interface without mixing and a region with some local mixing. The five equation two-dimensional model of Guillard-Murrone [9] has been applied in a large set of two-dimensional test cases. The purpose of the present work is to extend the two-dimensional model of Guillard-Murrone to three dimensions using unstructured tetrahedra volumes. The scheme is implemented in the basic solver in the AERO code developed at the University of Colorado by Farhat [6] with the collaboration of INRIA - see Dervieux [5], Nkonga and Guillard [1], and Martin and Guillard [14] for fluid flow problems.

2 Numerical Algorithm

An important reason for selecting the AERO code for integrating the recent two-phase advancements of the SMASH team (see Murrone and Guillard [10], and Murrone [17]) into a three-dimensional code is that the integration is facilitated by the fact that the origins of the two-dimensional code of Murrone and Guillard are an earlier 2D version of the AERO code.

The fluid part of the software AERO-F has been extended to the calculation of two-phase flows replacing the Euler equations for a unique perfect gas by the following two-phase model[1]:

[1]The term "two-phase flows" is used in the literature to describe flows involving two different liquids or gases: examples, liquid and gas, or two different liquids as in the present report. If the fluids change physical state for example, liquid changing to gas or vice versa, the term "two-phase reacting flows" is used. Both reacting and non-reacting two-phase flows have the same feature, that is, the computation of the interface separating the two liquids.

Seven-equation quasi conservative reduced model

$$\frac{\partial}{\partial t}\alpha_k\rho_k + \mathrm{div}(\alpha_k\rho_k u) = 0\ ;\quad k=1,2 \tag{1}$$

$$\frac{\partial}{\partial t}\rho u + \mathrm{div}(\rho u\otimes u) + \nabla p = 0 \tag{2}$$

$$\frac{\partial}{\partial t}\rho e + \mathrm{div}(\rho e + p)u = 0 \tag{3}$$

$$\frac{\partial}{\partial t}\alpha_2 + u\dot{\nabla}\alpha_2 = \alpha_1\alpha_2\frac{\rho_1 a_1^2 - \rho_2 a_2^2}{\sum_{k=1}^{2}\alpha_{k'}\rho_k a_k^2}\mathrm{div}u \tag{4}$$

with $e = \varepsilon + u^2/2$ and $\rho\varepsilon = \sum_{k=1}^{2}\alpha_k\rho_k\varepsilon_k(p,\rho_k)$.

where α_k are the mass fractions of the two fluids, ρ_k the corresponding densities, u, p the velocity and pressure common to the two phases.

2.1 Finite-volume approximation

A vertex-centred finite-volume approximation on a dual mesh constructed from a finite-element discretization of the computational domain by triangles (2D) or tetrahedra (3D) is used in this work.

In the 2D case, the cells are delimited by the triangle medians (see Figure 1). In 3D the cells are delimited by planes bisecting the edges of the tetrahedra comprising the cells.

Integrating Equations (1-4) over a cell Ω_i (see Figure 2) using a conservative approximation in terms of the dependent variables leads to the following semi-discretization of Equations (1-4):

$$a_i\,\frac{dU_i}{dt} + \sum_{j\in V(i)}\Phi(U_i,U_j,\nu_{ij}) = 0 \tag{5}$$

where a_i is the area (2D) or volume(3D) of the cell Ω_i. $V(i)$ is the set of nodes connected to node i (cell center), and $\nu_{ij} = \int_{\partial\Omega_{ij}}\mu_{ij}\,ds$. μ_{ij} denotes the

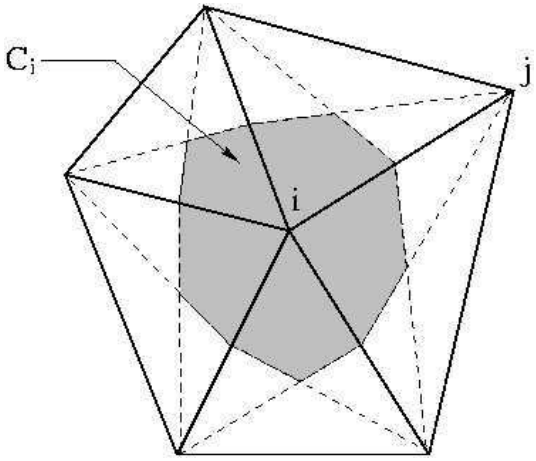

Figure 1: Finite-volume cell (2D case)

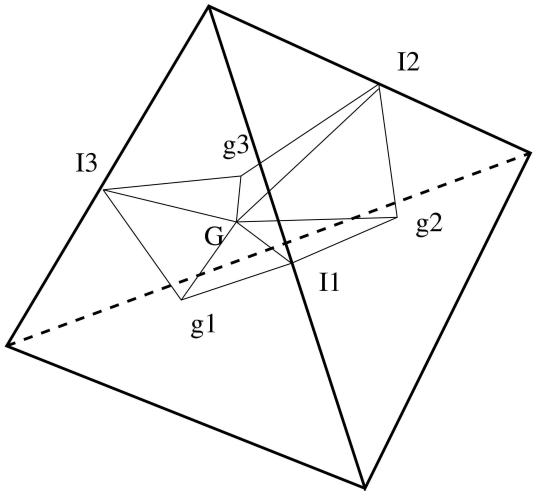

Figure 2: Cell boundary inside a tetrahedron between cells i and j (3D case): i and j is the centroids of elements and g_i are centroids of faces

unitary normal to the boundary $\partial\Omega_{ij} = \partial\Omega_i \cap \partial\Omega_j$ shared by the cells Ω_i and Ω_j.

In the above semi-discretization, the values U_i and U_j correspond to a constant per cell *interpolation* of the variable U, and Φ is a **numerical flux**

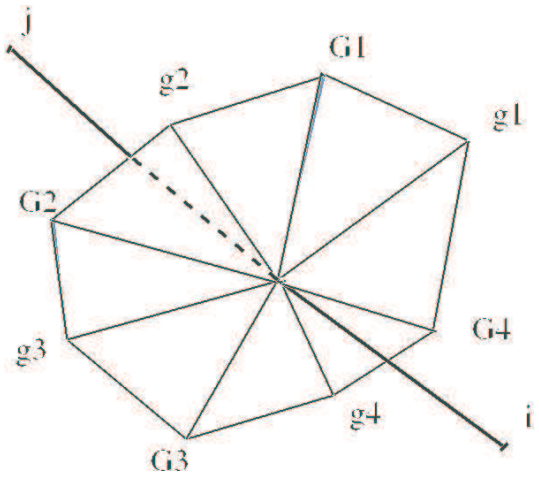

Figure 3: Cell interface between cells i and j (3D case): i and j is the centroids of elements and g_i are centroids of faces

function so that $\Phi(U_i, U_j, \nu_{ij})$ approximates $\int_{\partial\Omega_{ij}} \mathcal{F}(U) \cdot \mu_{ij}(s)ds$.

In general, the numerical flux function $\Phi : (u, v, \nu) \rightarrow \Phi(u, v, \nu)$ is assumed to be Lipschitz continuous, monotone increasing with respect to u, monotone decreasing with respect to v, and consistent

$$\Phi(u, u, \nu) = \mathcal{F}(u) \cdot \nu \tag{6}$$

We consider in the next section the definition of the flux function for the seven-equation model.

2.2 Acoustic approximate Riemann Solver

The acoustic solver for the five equation two phase flows model was developped in [18] and can be understood as an extension of the acoustic solver described for instance in [22] for the Euler equations of gas dynamics. This linearized Riemann solver uses strongly the mathematical structure of the model and in particular the continuity of pressure and velocity across a contact discontinuity. With respect to the different numerical test, this acoustic solver seems to be very robust with respect to the Mach number and specially for interface problems (see [16]). The principle of this solver is to write linearized

characteristic equations starting on the two side of the discontinuity and to compute their intersection to get the velocity and pressure at the interface. To be more specific we first transform the system of partial differential equations into ordinary differential equations by multiply them with the left eigenvectors :

$$ {}^t l_i(\mathbf{q}) \cdot (\frac{\partial \mathbf{q}}{\partial t} + A(\mathbf{q}) \frac{\partial \mathbf{q}}{\partial x}) = 0 \tag{7} $$

which can be immediately rewritten :

$$ {}^t l_i(\mathbf{q}) \cdot (\frac{\partial \mathbf{q}}{\partial t} + \lambda_i(\mathbf{q}) \frac{\partial \mathbf{q}}{\partial x}) = 0 \tag{8} $$

Note that $\mathbf{q} = {}^t(s_1, s_2, \mathbf{u}, p, Y_1)$ is the "entropic' vector variables. Now, denoting q_L^*, q_R^*, respectively the states on the left and right side of the contact discontinuity and linearizing (8) with respect to q_L and q_R we get

$$ \left\{ \begin{array}{l} {}^t l_{u+\hat{a}}(\mathbf{q}_L) \cdot (\mathbf{q}_L^* - \mathbf{q}_L) = 0 \\ \\ {}^t l_{u-\hat{a}}(\mathbf{q}_R) \cdot (\mathbf{q}_R^* - \mathbf{q}_R) = 0 \end{array} \right. \tag{9} $$

which gives after some algebraic manipulations :

$$ \left\{ \begin{array}{l} \rho_L \hat{a}_L (u_L^* - u_L) + (p_L^* - p_L) = 0 \\ \\ \rho_R \hat{a}_R (u_R^* - u_R) - (p_R^* - p_R) = 0 \end{array} \right. \tag{10} $$

Then using the fact that $u_L^* = u_R^* = u^*$ and $p_L^* = p_R^* = p^*$, we get the following expressions for u^* and p^* :

$$ \left\{ \begin{array}{l} u^* = \dfrac{\rho_L \hat{a}_L u_L + \rho_R \hat{a}_R u_R}{\rho_L \hat{a}_L + \rho_R \hat{a}_R} - \dfrac{p_R - p_L}{\rho_L \hat{a}_L + \rho_R \hat{a}_R} \\ \\ p^* = \dfrac{\rho_R \hat{a}_R p_L + \rho_L \hat{a}_L p_R}{\rho_L \hat{a}_L + \rho_R \hat{a}_R} - \dfrac{\rho_L \hat{a}_L \rho_R \hat{a}_R (u_R - u_L)}{\rho_L \hat{a}_L + \rho_R \hat{a}_R} \end{array} \right. \tag{11} $$

And finally the solution of the Riemann's problem is given by :

$$\mathbf{q}(\frac{x}{t},\mathbf{q}_L,\mathbf{q}_R) = \begin{cases} \mathbf{q}_L & \text{if} \quad \frac{x}{t} < u_L - \hat{a}_L \\ \mathbf{q}_L^* & \text{if} \quad u_L - \hat{a}_L < \frac{x}{t} < u^* \\ \mathbf{q}_R^* & \text{if} \quad u^* < \frac{x}{t} < u_R + \hat{a}_R \\ \mathbf{q}_R & \text{if} \quad u_R + \hat{a}_R < \frac{x}{t} \end{cases} \tag{12}$$

2.3 Higher-order spatial accuracy

Higher-order schemes are derived according to the MUSCL method of van Leer [23]. This is best explained with the aid of Figure 4 (2D case) which shows an edge (or segment) between the control-volume centers i and j. The interface between the two control volumes bisects the segment ij. The interface values for the segment ij are denoted by U_{ij} for the control volume centered at i and U_{ji} for the control volume centered j and U_{ji}

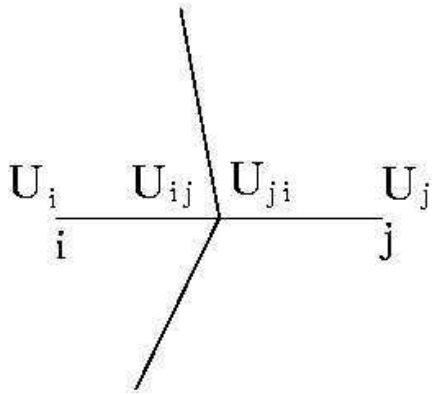

Figure 4: Interface values

In the MUSCL approach, the order of space-accuracy is improved by substituting in the numerical flux function higher-order interpolations U_{ij} and U_{ji} at the interface $\partial\Omega_{ij}$.

$$a_i \frac{dU_i}{dt} + \sum_{j \in V(i)} \Phi(U_{ij}, U_{ji}, \nu_{ij}) \; = \; 0 \tag{13}$$

where U_{ij} and U_{ji} are interface values of U $\partial\Omega_{ij}$ obtained by higher-order interpolation.

$$U_{ij} = U_i + \frac{1}{2}\Delta s_{ij} \vec{\nabla} W_i \cdot \nu_{ij} \tag{14}$$

$$U_{ji} = U_j + \frac{1}{2}\Delta s_{ij} \vec{\nabla} W_j \cdot \nu_{ij} \tag{15}$$

where Δs_{ij} is the distance between the i and j vertices.

The first-order scheme is obtained by taking $U_{ij} = U_i$ and $U_{ji} = U_j$. Second-order accuracy spatial accuracy is achieved using either 1) the nodal gradient approach or, 2) the upwind tetrahedra method of Fezoui and Dervieux in [7].

The nodal gradient $\left(\vec{\nabla} W\right)_i$ is calculated as the average of the gradients on tetrahedra $T \in C_i$ having the node i as a vertex:

$$\left(\vec{\nabla} W\right)_i = \frac{1}{Vol(C_i)} \sum_{T \in C_i} \frac{Vol(T)}{3} \sum_{k \in T} W_k \vec{\nabla} \Phi_k^T \tag{16}$$

In order to keep the scheme non oscillatory and positive, **limiters** are introduced. It has been early proved that higher-order positive schemes must be built with a nonlinear process - see Harten [11]. In the case of unstructured meshes and scalar models, second-order positive schemes were derived using a two-entry symmetric limiter by Jameson in [12]. Here, instead of a symmetric limiter, we choose a MUSCL formulation (involving two limiters per edge) according to Van Leer [23]. The adaptation to triangulations is close to the one proposed in [7] and [21].

From the upwind schemes proposed by these authors, we introduce three-entry limiters, following [4]; this allows us to design a positive scheme, of third-

(or even fifth-) order far from extrema when U varies smoothly.

For **stationary grids** the seven-equation model has the form

$$a_i \frac{dU_i}{dt} + \sum_{j \in V(i)} \Phi(U_i + \frac{1}{2} L_{ij}(U), U_j + \frac{1}{2} L_{ji}(U), \nu_{ij}) \; = \; 0, \tag{17}$$

Higher-order accuracy using inflow/outflow tetrahedra: In order to define $L_{ij}(U)$ and $L_{ji}(U)$ we use the downstream and upstream triangles (or tetrahedra) T_{ij} and T_{ji} (see Figure 5 for the 2D case), as introduced by Fezoui and Dervieux in [7]. We denote

$$\Delta^- U_{ij} \; = \; \vec{\nabla} U \, |_{T_{ij}} \cdot \vec{ij} \quad , \quad \Delta^0 U_{ij} = U_j - U_i \quad and \quad \Delta^- U_{ji} \; = \; \vec{\nabla} U \, |_{T_{ji}} \cdot \vec{ij} \, ,$$

where the gradients are those of the P1 (continuous and linear) interpolation of U.

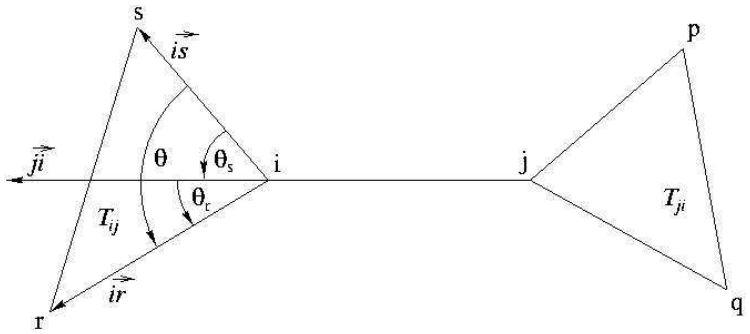

Figure 5: Downstream and Upstream Triangles (2D case)

Jameson in [12] has noted that for the 3D case

$$\Delta^- U_{ij} \; = \; \epsilon_{ri} \, (U_i \, - \, U_r) \, + \, \epsilon_{si} \, (U_i \, - \, U_s) \, + \, \epsilon_{ti} \, (U_i \, - \, U_t) \, ,$$

and

$$\Delta^- U_{ji} \; = \; \epsilon_{jn} \, (U_n \, - \, U_j) \, + \, \epsilon_{jp} \, (U_p \, - \, U_j) \, + \, \epsilon_{jq} \, (U_q \, - \, U_j) \, ,$$

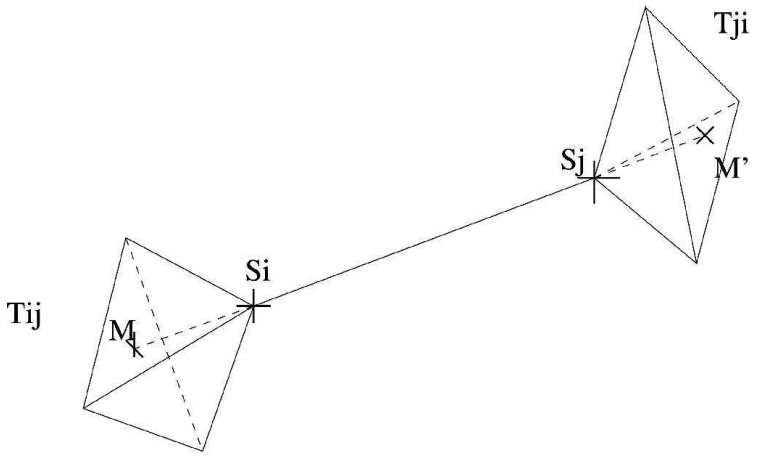

Figure 6: Downstream and Upstream Tetrahedra (3D case)

where the coefficients ϵ_{ri}, ϵ_{si}, ϵ_{ti}, ϵ_{jn}, ϵ_{jp} and ϵ_{jq} are all positive, possibly zero (t and n correspond to the third dimension).

Now, we introduce a family of continuous limiters with three entries, satisfying

$(P1)$ $L(u,v,w) = L(v,u,w)$

$(P2)$ $L(\alpha\, u, \alpha\, v, \alpha\, w) = \alpha\, L(v,u,w)$

$(P3)$ $L(u,u,u) = u$

$(P4)$ $L(u,v,w) = 0$ if $uv \leq 0$

$(P5)$ $0 \leq \frac{L(u,v,w)}{v} \leq 2$ if $v \neq 0$.

As an example, we consider the following limiter

$$\begin{cases} L(u,v,w) = 0 & \text{if } uv \leq 0 \\ \qquad\qquad = Sign(u)\, \min(\, 2\,|u|\,,\, 2\,|v|\,,\, |w|) & \text{otherwise.} \end{cases} \tag{18}$$

We define:

$$L_{ij}(U) = L(\Delta^{-}U_{ij}\,,\, \Delta^{0}U_{ij}\,,\, \Delta^{HO}U_{ij}) \;\;;\;\; L_{ji}(U) = L(\Delta^{-}U_{ji}\,,\, \Delta^{0}U_{ji}\,,\, \Delta^{HO}U_{ji}). \tag{19}$$

When $L_{ij}(U) = 0$, we switch to the first-order MEV scheme and when the limitation is not active, $L_{ij}(U) = \Delta^{HO} U_{ij}$, so that the scheme is of higher-order spatial-accuracy.
We take

$$\Delta^{HO} U_{ij} = \frac{1}{3}\,\Delta^{-} U_{ij} + \frac{2}{3}\,\Delta^{0} U_{ij}\,, \tag{20}$$

which gives us a third-order space-accurate scheme for linear advection on cartesian triangular meshes (see [3]).

Equation (19) allows for some positiveness properties described in [2].

2.4 Time accuracy

A positive scheme can be advanced in time by a multistage positivity preserving scheme; this idea dates back to the works of Shu, cf. [20]. A general high-order explicit time discretization can be written in the form:

$$\left\{ \begin{array}{rcl} U_i^{(0)} & = & U_i^n \\ U_i^{(j)} & = & \sum_{k=0}^{j-1} \left(\alpha_{jk} U_i^{(k)} + \Delta t\, \beta_{jk} L(U^{(k)}) \right) \quad j = 1, \ldots, m \\ U_i^{(m)} & = & U^{n+1} \end{array} \right.$$

with $\displaystyle\sum_k \alpha_{jk} = 1$ for consistency.
If all the coefficients α_{jk} and β_{jk} are non-negative, $U^{(j)}$ is a convex combination of terms in the form:

$$U_i^{(k)} + \Delta t\ \frac{\beta_{jk}}{\alpha_{jk}}\ L(U^{(k)})$$

They correspond to first-order time discretizations with time steps equal to $\left(\Delta t\, \dfrac{\beta_{jk}}{\alpha_{jk}} \right)$ and thus are positive provided that:

$$b_i\, \Delta t\, \frac{\beta_{jk}}{\alpha_{jk}} \geq 1 \text{ for all } j \text{ and } k\ .$$

In particular, we choose the third-order time discretization given in [20]:

$$\left\{ \begin{array}{rcl} U_i^{(1)} & = & U_i^n + \Delta t\, L(U^n) \\ U_i^{(2)} & = & \frac{3}{4}U_i^n + \frac{1}{4}U_i^{(1)} + \frac{1}{4}\Delta t\, L(U^{(1)}) \\ U_i^{n+1} & = & \frac{1}{3}U_i^n + \frac{2}{3}U_i^{(2)} + \frac{2}{3}\Delta t\, L(U^{(2)}) \end{array} \right.$$

We have $\min_{j,k} \frac{\beta_{jk}}{\alpha_{jk}} = 1$ and the CFL condition to preserve positivity for this third-order time discretization is the same as for the first-order one.

3 Numerical results

3.1 Falling water column

Shown in Figures 8-12 are results for the falling water column test case of Moyce [15] et al. and the computational results of Lesage, Allain, and Dervieux [13] using a level set method. The 3D computations used a mesh of 101x101x3 vertices in the x, y, z directions. The 2D results were computed using 101x101 vertices in the x, y directions. We compare the results using the five equation two-dimensional model of Guillard-Murrone [9], the seven equation three-dimensional model, and the experimental data of Moyce [15]. These results are in good global agreement - the deviation between the computational results and the experiments are coherent with other computations reported in the literature.

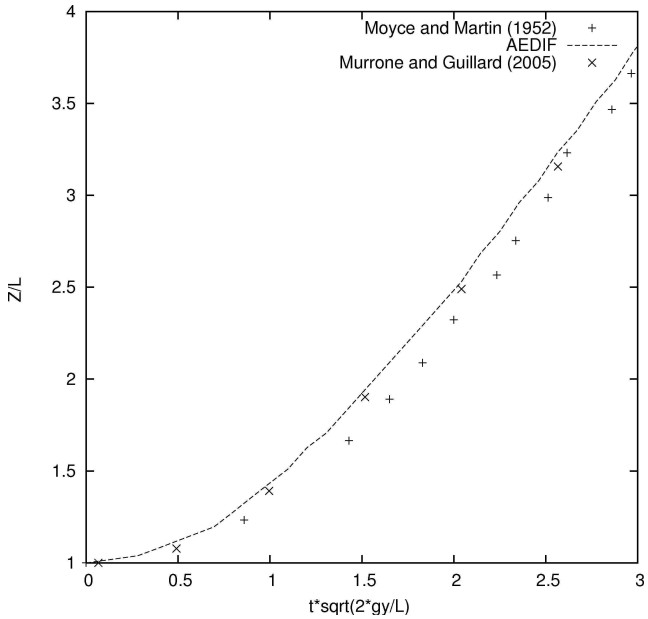

Figure 7: 2D Water column under gravity: Comparison with data

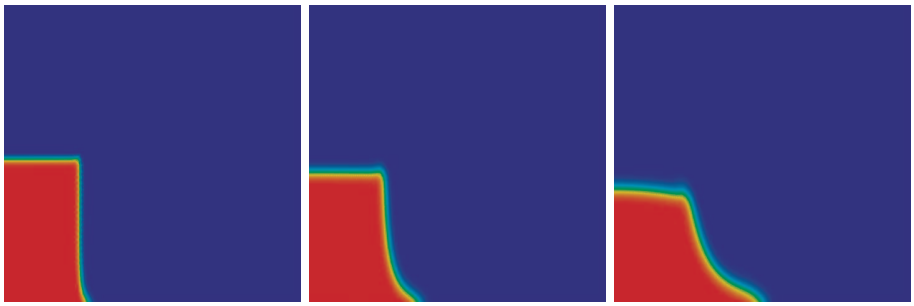

Figure 8: AEDIF - Water column: t $\star\sqrt{2\star g/L} = 0.491, \quad 0.995, \quad 1.517$

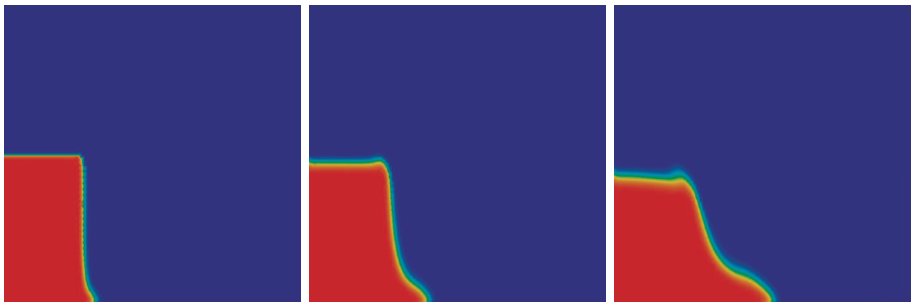

Figure 9: 2D code - Water column: t $\star\sqrt{2\star g/L} = 0.491, \quad 0.995, \quad 1.517$

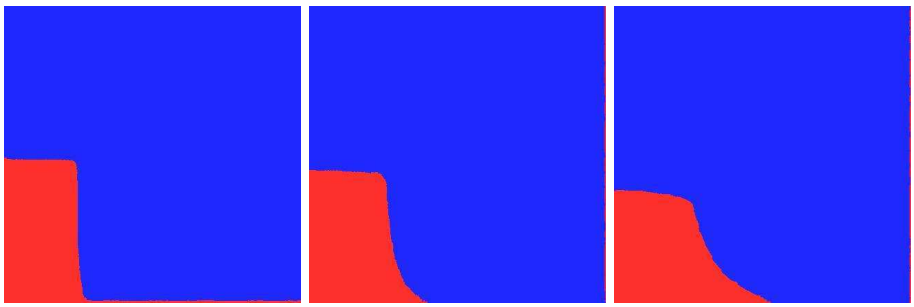

Figure 10: 3D Level Set code - Water column: t $\star\sqrt{2\star g/L} = 0.491, \quad 0.995, \quad 1.517$

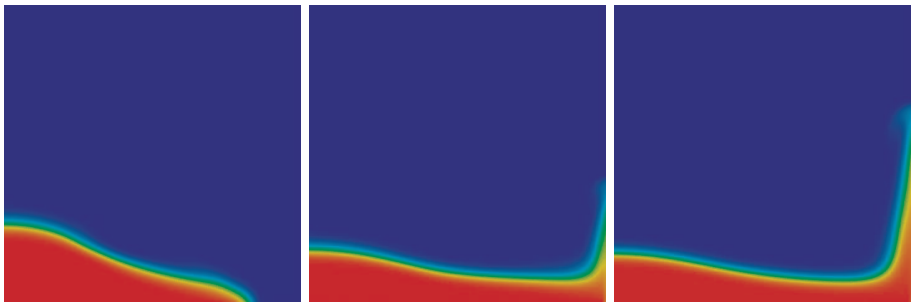

Figure 11: AEDIF - Water column: t $\star\sqrt{2\star g/L}$ = 2.566, 3.586, 4.103

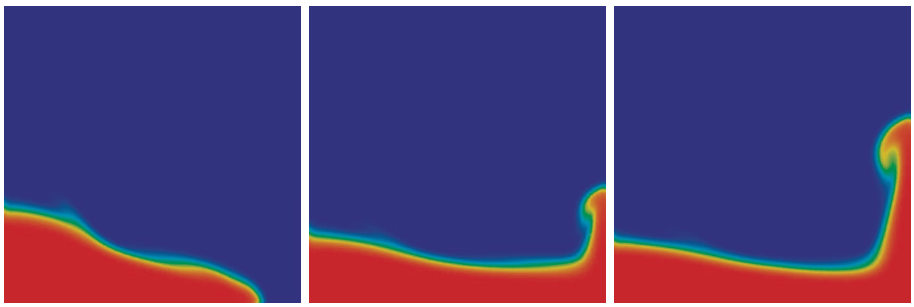

Figure 12: 2D code - Water column: t $\star\sqrt{2\star g/L}$ = 2.566, 3.586, 4.103

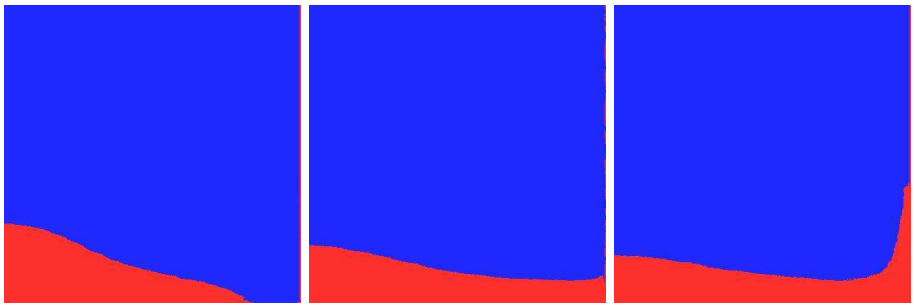

Figure 13: 3D Level Set code - Water column: t $\star\sqrt{2\star g/L}$ = 2.566, 3.586, 4.103

3.2 Blast wave-bubble interaction

This kind of flow has been studied in 2D and 2D axisymmetric computations by Giordano [8]. Very fine 3D calculations are necessary in order to study unstable capillary effects. The present calculations are a step in this direction.

The initial pressure ratio across the blast wave is 10/1. The initial ratio of the density inside the sphere to the exterior is 10/1. The initial velocity was zero for the entire field. The explicit three-stage time scheme was used to advance the solution in time.

Figures 14-16 show snapshots of the density, pressure, and pressure contours for the plane x = 1/2 [2] at time steps 0, 100, 200, 300, 400, 500, 600, and 700. The initial positions of the blast wave and sphere can be seen in the snapshot (far left of the figures).

At time step 100, the blast wave has advanced upward creating a density layer visible in Figure 14. An expansion wave propagates toward the bottom of the figure creating a downward velocity. The blast wave creates an equal velocity in the vertical direction.

Time step 300 shows the solution after the expansion has reflected off the lower boundary creating a velocity in the opposite direction from that created before the reflection. The result being a cancellation of the velocity field. At time step 300, the blast wave has past through the sphere introducing a small upward vertical velocity to the liquid inside the sphere while greatly accelerating the fluid exterior of the sphere. The density increases inside the sphere as the blast wave passes through it. Time steps 400-700 show the contours before and after the reflection of the bast wave from the upper boundary.

[2]The min/max values of x, y, z ranges are (0-1), (0-1), and (0-2).

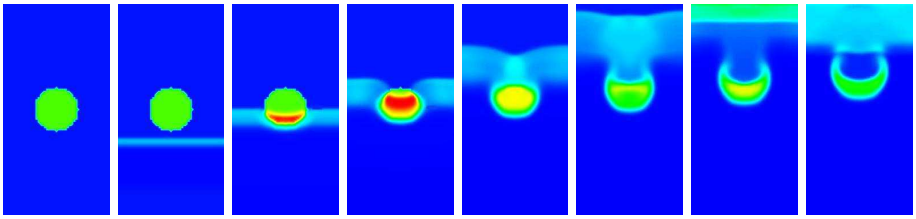

Initial 100 200 300 400 500 600 700

Figure 14: x = 1/2 plane: Snapshot of Density contours in time

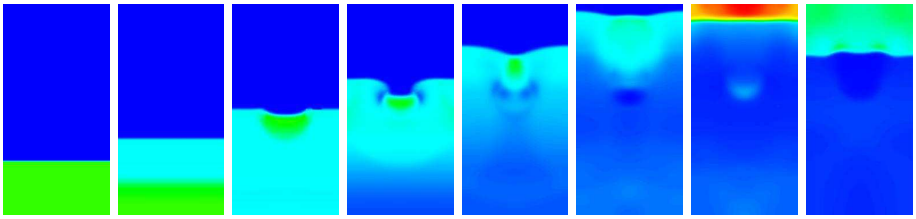

Initial 100 200 300 400 500 600 700

Figure 15: x = 1/2 plane: Snapshot of Pressure contours in time

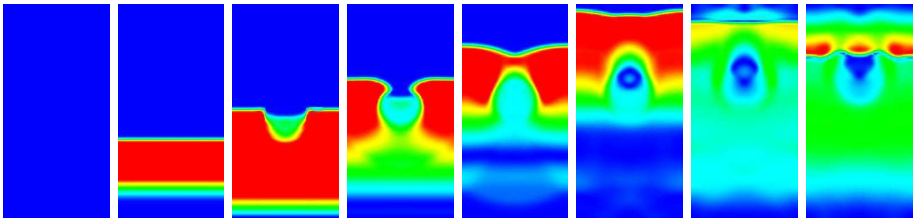

Initial 100 200 300 400 500 600 700

Figure 16: x = 1/2 plane: Snapshot of Velocity magnitude contours in time

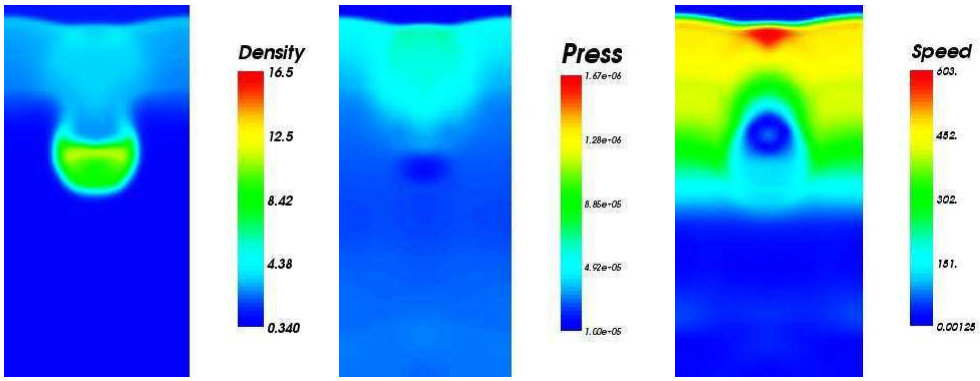

Figure 17: Left) Density, Center) Pressure, Right) Velocity Magnitude

Figure 17 shows the contour levels for the snapshot figures and the contours at time step 500. Shown in Figure 18 are the contours of the Mach number; Left, shows the three-dimensional Mach contours and Right, the Mach contours on the x = 1/2 plane and the three-dimensional $\alpha = 1/2$ contour colored by the Mach number.

Figure 19 show the three-dimensional density contours after 720 time steps at which time the blast wave has passed through the bubble reflected off the top boundary and passed through the bubble a second time.

4 Conclusion

We have presented the extension of the five-equation two-dimensional two-phase model of Guillard and Murrone to three-dimensions. The Riemann solver is the acoustic version of the one proposed by Guillard and Murrone. The numerical scheme is a Mixed-Element-Volume approximation centered on the vertices of a tetrahedrization. It uses an edge based formulation. Upstream-Downstream tetrahedra-based limiters are applied for positiveness reinforcement. The computation in advanced in time using explicit multi-stage schemes. This numerical technology is implemented in the parallel mode using mesh partitioning and the message passing interface (MPI). Further adaption to parallel grid computations are reported by Wornom [24] [25]. The new scheme is stable, produces smooth results and compares well with other results reported in

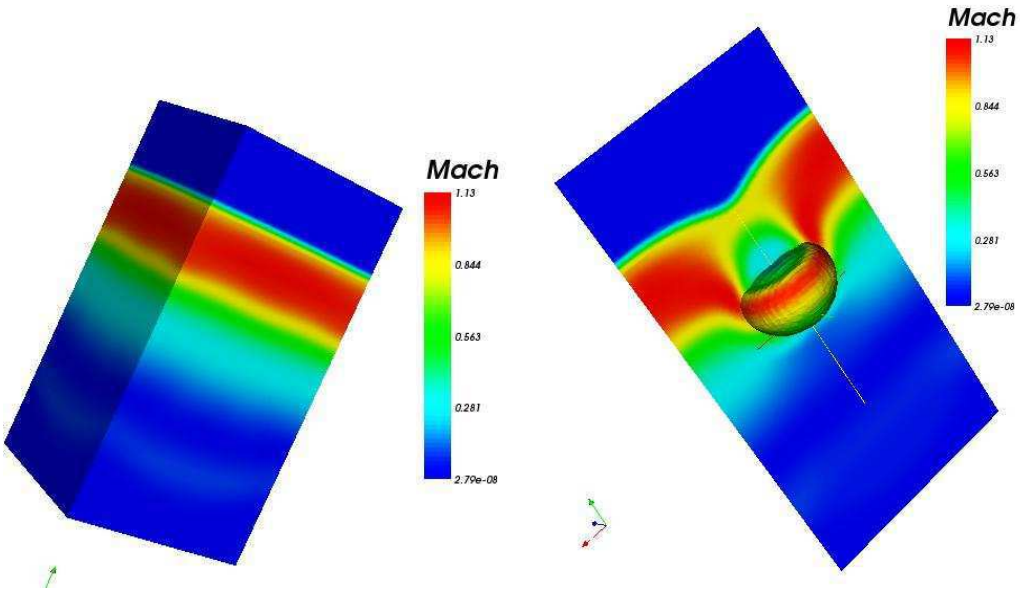

Figure 18: Mach contours at time step 500: Left) Three-dimensional, Right) x = 1/2 plane

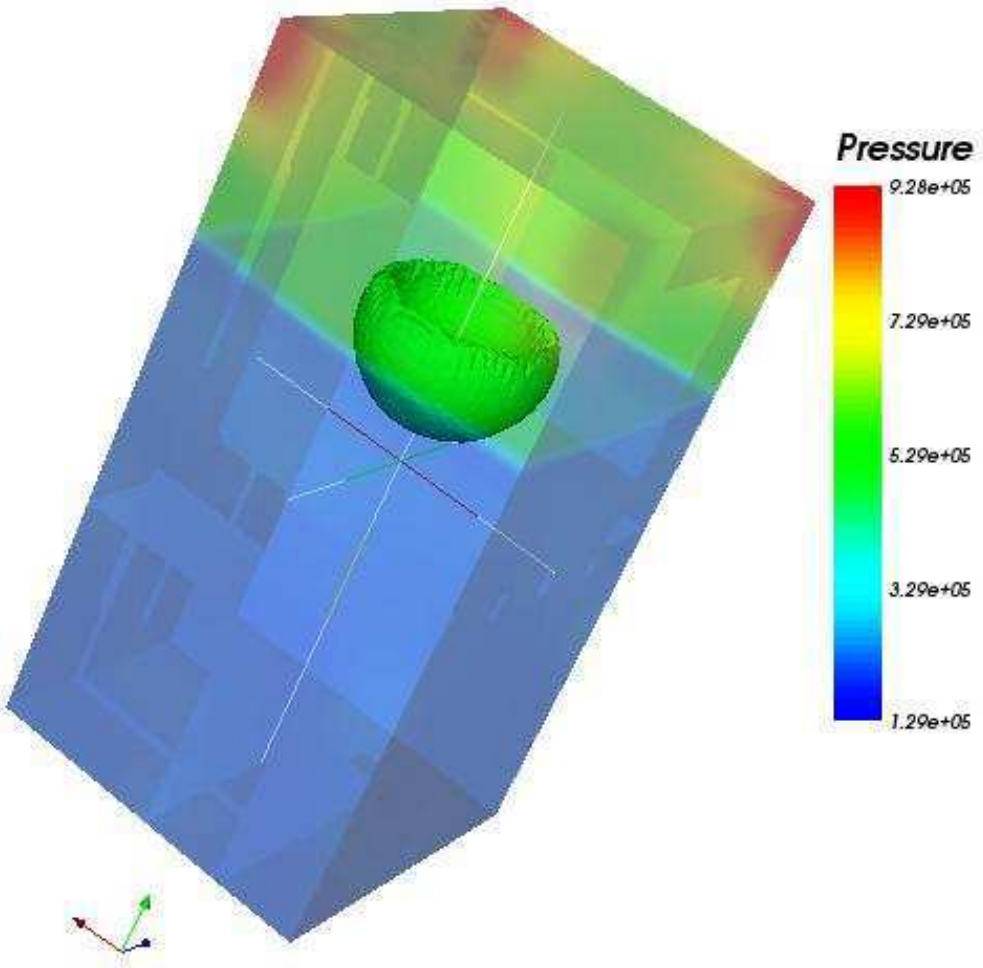

Figure 19: Blast wave pressure contours after 720 time steps

the literature. Future research will concern further experiments with bubbles and modeling of capillary flows.

5 Acknowledgements

The research has been made possible by the ACI-GRID 2002 Project of the French Ministry of Research[3]. The authors would like to acknowledge the support of Centre Informatique National de l'Enseignement Supérieur (CINES[4]), Montpellier, FRANCE.

[3]http://www.recherche.gouv.fr/recherche/aci/grid.htm
[4]http://www.cines.fr

References

[1] B. Nkonga and H. Guillard. Godunov type method on non-structured meshes for three dimensional moving boundary problems. *Comput. Methods Appl. Mech. Eng*, 113:183–204, 1994.

[2] P.-H. Cournède, B. Koobus, and A. Dervieux. Positivity statements for a mixed-element-volume scheme on fixed and moving grid. *submitted to Revue Européenne des Eléments Finis*, , 2005.

[3] C. Debiez and A. Dervieux. Mixed element volume muscl methods with weak viscosity for steady and unsteady flow calculation. *Computer and Fluids*, 29:89–118, 1998.

[4] Ch. Debiez. *Approximation et linéarisation d'écoulements aérodynamiques instationnaires*. PhD thesis, Université de Nice, France, 1996.

[5] A. Dervieux. Steady Euler simulations using unstructured meshes. Lecture series 1985-04[5], Von Karman Institute for Fluid Dynamics, 1985.

[6] C. Farhat. High performance simulation of coupled nonlinear transient aeroelastic problems. Special course on parallel computing in CFD. R-807, NATO AGARD Report, October 1995.

[7] L. Fezoui and A. Dervieux. Finite-element non oscillatory schemes for compressible flows. *Symposium on Computational Mathematics and Applications, Pavie*, (730), 1989.

[8] J. Giordano. *Contribution à la modelélisation numérique des problèmes d'interactions fluide-fluide et fluide-structure*. PhD thesis, Université d'Aix-Marseille I, 2004.

[9] H. Guillard and A. Murrone. A five equation reduced model for compressible two phase flow problems. Technical Report RR-4778, INRIA - Sophia Antipolis, Mars 2003.

[10] H. Guillard and A. Murrone. A five equation reduced model for compressible two phase flow problems. Technical Report RR-4778, INRIA - Sophia

[5] Published in Partial Differential Equations of hyperbolique type and Applications, Geymonat Ed., World Scientific (1987)

Antipolis, March 2003, accepted for publication in Journal of Computational Physics, available at http://www.inria.fr/rrrt/rr-4778.html.

[11] A. Harten. High resolution schemes for hyperbolic conservation laws. *Journal of Computational Physics*, 49, 357-393 (1983).

[12] A. Jameson. Artificial Diffusion, Upwind Biasing, Limiters and their Effect on Accuracy and Multigrid Convergence in Transonic and Hypersonic Flows. *AIAA paper 1993-3359*.

[13] A. C. Lesage, O. Allain, and A. Dervieux. A numerical accuracy study for level set formulations, June 21-25, Porquerolles, France.

[14] R. Martin and H. Guillard. Second-order defect-correction scheme for unsteady problems. *Computer & Fluids.*, 25(1):9–27, 1996.

[15] W. J. Moyce and J. C. Martin. An experimental study of the collapse of liquid columns on a rigid horizonal plane. *Philos. Trans. Roy. Soc. London*, A244:312–324, 1952.

[16] A. Murrone. *Modèles bi-fluides à six et sept équations pour les écoulements diphasiques à faible nombre de Mach*. PhD thesis, University of Aix-Marseille I, to be found at http://tel.ccsd.cnrs.fr/, 2003.

[17] A. Murrone. *Modèles bi-fluides à six et sept équations pour les écoulement diphasiques à faible nombre de Mach*. PhD thesis, Université de Provence (Aix-Marseille I), 2004, available at http://www.ccsd.crns.fr.

[18] A. Murrone and H. Guillard. A five equation reduced model for compressible two phase flow problems. *Journal of Computational Physics*, 202:664–698, 2005.

[19] R. Saurel and R. Abgrall. A simple method for compressible multifluid flows. *SIAM J. Sci. Comput.*, 21-3:1115–1145, 1999.

[20] C. W. Shu and S. Osher. Efficient implementation of essential non-oscillatory shock capturing schemes. *Journal of Computational Physics*, 77(439-471), 1988.

[21] B. Stoufflet, J. Periaux, L. Fezoui, and A. Dervieux. 3-d hypersonic Euler numerical simulation around space vehicles using adapted finite elements. *25th AIAA Aerospace Meeting, Reno NV, AIAA Paper 86-056*, 1987.

[22] E. F. Toro. *Riemann Solvers and numerical methods for fluid dynamics.* Springer Verlag, Berlin, 1997.

[23] B. van Leer. Towards the ultimate conservative difference scheme V: a second-order sequel to Godunov's method. *J. Comp. Phys.*, 32:361–370, 1979.

[24] S. Wornom. Parallel computations of one-phase and two-phase flows using the MecaGRID. Technical Report RT-297, INRIA - Sophia Antipolis, August 2004.

[25] S. Wornom. Optimizing a CFD fortran code for GRID Computing. Technical Report RT-303, INRIA - Sophia Antipolis, April 2005.

Unité de recherche INRIA Sophia Antipolis
2004, route des Lucioles - BP 93 - 06902 Sophia Antipolis Cedex (France)

Unité de recherche INRIA Futurs : Parc Club Orsay Université - ZAC des Vignes
4, rue Jacques Monod - 91893 ORSAY Cedex (France)
Unité de recherche INRIA Lorraine : LORIA, Technopôle de Nancy-Brabois - Campus scientifique
615, rue du Jardin Botanique - BP 101 - 54602 Villers-lès-Nancy Cedex (France)
Unité de recherche INRIA Rennes : IRISA, Campus universitaire de Beaulieu - 35042 Rennes Cedex (France)
Unité de recherche INRIA Rhône-Alpes : 655, avenue de l'Europe - 38334 Montbonnot Saint-Ismier (France)
Unité de recherche INRIA Rocquencourt : Domaine de Voluceau - Rocquencourt - BP 105 - 78153 Le Chesnay Cedex (France)

Éditeur
INRIA - Domaine de Voluceau - Rocquencourt, BP 105 - 78153 Le Chesnay Cedex (France)
http://www.inria.fr
ISSN 0249-6399